

# VOBOZ: An Almost-Parameter-Free Halo-Finding Algorithm

Mark C. Neyrinck<sup>1,3</sup>, Nickolay Y. Gnedin<sup>2,3</sup>, and Andrew J.S. Hamilton<sup>1,3</sup>

<sup>1</sup>*JILA, University of Colorado, Boulder, CO 80309*

<sup>2</sup>*Center for Astrophysics and Space Astronomy, University of Colorado, Boulder, CO 80309*

<sup>3</sup>*Department of Astrophysical and Planetary Sciences, University of Colorado, Boulder, CO 80309*

*email: Mark.Neyrinck@colorado.edu*

2004 July 6

## ABSTRACT

We have developed an algorithm to find haloes in an  $N$ -body dark matter simulation, called VOBOZ (Voronoi Bound Zones), which has as little dependence on free parameters as we can manage. By using the Voronoi diagram, we achieve nonparametric, ‘natural’ measurements of each particle’s density and set of neighbors. We then eliminate much of the ambiguity in merging sets of particles together by identifying every possible density peak, and measuring the probability that each does not arise from Poisson noise. The main halo in a cluster tends to have a high probability, while its subhaloes tend to have lower probabilities. The first parameter in VOBOZ controls the subtlety of particle unbinding, and may be eliminated if one is cavalier with processor time; even if one is not, the results saturate to the parameter-free answer when the parameter is sufficiently small. The only parameter which remains, an outer density cut-off, does not influence whether or not haloes are identified, nor does it have any effect on subhaloes; it only affects the masses returned for supercluster haloes.

**Key words:** methods:  $N$ -body simulations – large-scale structure of Universe – galaxies: haloes – cosmology: theory – methods: data analysis – galaxies: formation.

## 1 INTRODUCTION

A crucial step in comparing  $N$ -body simulations to the observed galaxy distribution is to identify the possible sites of galaxy formation, called dark-matter haloes, in the simulations. Unfortunately, the concept of a dark-matter halo is not precisely defined. There is no firm observational definition of dark-matter haloes, since they can only be observed indirectly; for example, through gravitational lensing. There are a couple of possible theoretical definitions. One of them is a region exceeding a certain overdensity, such as the canonical overdensity of virialization, 200. This is often used when seeking Halo Occupation Distributions (e.g. Berlind & Weinberg 2002), which statistically characterize the number of galaxies inside haloes (implicitly dark-matter hereafter) as a function of halo mass. However, if we want to look beyond the statistical placement of galaxies inside haloes, we should use another definition of a halo (or subhalo): a density peak to which some mass is gravitationally bound. In the language of an  $N$ -body simulation, a particle is the core of a halo if it is a local density maximum, and there exists at least one other particle bound to it.

One of the first halo-finding algorithms (HFAs), still in wide use because it is so fast and conceptually simple, is the Friends-of-Friends algorithm (Davis et al. 1985). This

HFA groups together all particles within a specified linking length, a free parameter which is usually set by the canonical overdensity of virialization. Friends-of-Friends is useful if one is looking for large structures exceeding this overdensity, but it is incapable of finding subhaloes within these structures, and sometimes structures are unduly linked if there happens to be a stream of particles connecting them.

Most HFAs developed since Friends-of-Friends begin with an explicit measurement of the density, which is not uniquely or obviously defined given a set of particles. In one Eulerian method (DENMAX, Bertschinger & Gelb 1991), each particle is smoothed with a Gaussian of a fixed spatial resolution. As with the Friends-of-Friends algorithm, the free parameter is set roughly by the critical overdensity of virialization. While this value of the parameter tends to give virialized objects, it smears out subhaloes (Neyrinck, Hamilton & Gnedin 2004, hereafter NHG); one runs the risk of missing structures smaller than any fixed smoothing length. On the other hand, using a smoothing length that is too small misses the less-dense outskirts of haloes. Another HFA, called BDM (Klypin & Holtzman 1997), finds density maxima by placing spheres randomly in the simulation, and then moving them at each iteration to the center of mass of particles within them. Maxima are then joined if they lie within a specified

arXiv:astro-ph/0402346v3 6 Jul 2004

radius. Another way to find the density, called SKID (Weinberg, Hernquist & Katz 1997, Jang-Condell & Hernquist 2001) uses a Lagrangian, ‘smoothed particle hydrodynamics’ (SPH) density estimate based on the distances to the nearest  $N_{dens}$  particles. This density estimate is arguably an improvement over DENMAX’s because there is no fixed spatial resolution, but in its place there is an arbitrary, fixed mass resolution. This is undesirable because haloes can exist with only two particles, which a fixed mass resolution is likely to miss.

The next step in halo finding is to group the particles together. In DENMAX and SKID, particles slide along density gradients until they reach density maxima. In HOP (Eisenstein & Hut 1998), which uses a Lagrangian density estimator similar to that in SKID, each particle ‘hops’ to the densest particle among its neighbors, and continues in this manner until it reaches a local density maximum. Then, groups of particles are joined together if saddles linking them exceed a specified density, another free parameter. Recently, Kim & Park (2004) have developed another HFA, called PSB. Around each density maximum (calculated with a small spatial smoothing length), PSB finds the largest isodensity contour enclosing only that peak, using a couple of parameters to do so. It then assigns neighboring particles to density peaks using considerations such as whether they are energetically bound, and whether they lie outside the tidal radius. It seems that PSB reliably uncovers subhaloes, but it does require several free parameters.

## 2 METHOD

Our HFA, VOBOZ (VORONOI BOUND ZONES), identifies haloes in three steps: (1) measuring the density at each particle, (2) grouping sets of particles around density maxima which plausibly form a halo using only spatial information, and (3) unbinding particles from haloes if their velocities exceed the escape velocity from their halo at their position.

VOBOZ also performs a measurement new to the world of HFA’s: it measures the probability that each halo did not arise from Poisson noise. Such a measurement is quite useful for subhaloes within haloes which may or may not exist. Previous HFA’s either identify or do not identify questionable haloes; the results do not indicate haloes which were just barely identified, nor haloes which barely escaped detection.

### 2.1 Calculation of the Voronoi Diagram

The method we use to calculate the densities of particles employs the Voronoi diagram (VD), a unique, nonparametric tessellation of a space containing particles. Ideas related to the VD have existed for centuries, but Voronoi (1908) introduced it in its modern form. The standard reference is Okabe et al. (2000), in which appears a survey of Voronoi applications in an extensive array of fields including biology, forestry, archaeology, urban planning, and meteorology. A reference with a view toward astronomy is provided by van de Weygaert (1994), who, with his collaborators, has championed the use of Voronoi methods in various contexts related to large-scale structure and cosmology, starting with the description of voids as polyhedra (Icke & van de Weygaert

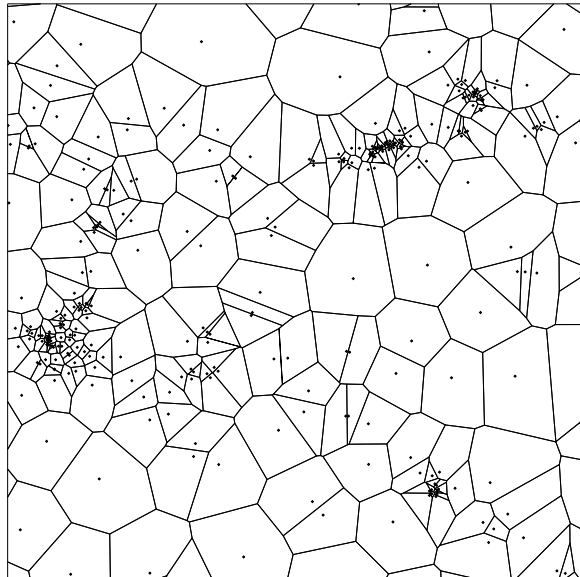


**Figure 1.** A two-dimensional Voronoi diagram of particles from an  $N$ -body simulation.

1987). A major current astronomical application of Voronoi methods is in identifying clusters of galaxies from surveys (e.g. Ebeling & Wiedenmann 1993, Ramella et al. 2001, Kim et al. 2002, Marinoni et al. 2002). The Delaunay Tessellation Field Estimator (Schaap & van de Weygaert 2000), essentially the same as our density estimator (it uses the dual of the VD, the Delaunay tessellation), has been shown to be superior to SPH (Pelupessy, Schaap & van de Weygaert 2003, Schaap 2004). Quite recently, Arad, Dekel & Klypin (2004) used the DTFE to explore the properties of 6-D position-velocity space in an  $N$ -body simulation.

The VD of a set of particles  $P$  is defined as follows. The Voronoi cell  $V(p_i)$  around a particle  $p_i$  in  $P$  is the interior of the polyhedron of points closer to  $p_i$  than to any other particle. The most intuitive way to find a Voronoi cell around  $p_i$  is, for each other particle  $p_j$  in  $P$ , to put up planes perpendicularly bisecting the line segments connecting  $p_i$  and  $p_j$ .  $V(p_i)$  will then be the polyhedron formed by these bisecting planes which contains  $p_i$ . Figure 1 shows a two-dimensional Voronoi diagram of a set of particles from an  $N$ -body simulation. A Voronoi neighbor, or adjacency, of a particle  $p_i$  is a particle  $p_j$  such that  $V(p_j)$  borders  $V(p_i)$ ; the set of Voronoi neighbors of  $p_i$  demarcate  $V(p_i)$ .

We may then define the density of a particle as  $1/\text{Volume}(V(p_i))$ . Not only does the VD give a unique density, with no free parameters, and with infinite spatial resolution, but it gives, arguably, the most local density estimate that contains meaningful information, uncovering every possible morsel of structure. It also returns a ‘natural’ set of neighbors for each particle, with no fixed mass resolution. In addition, it benefits from having been studied extensively. Many statistical properties of Poisson Voronoi diagrams (VD’s applied to Poisson point processes) are well-known, and sometimes are even analytically calculable. For example, the average number of neighbors of a particle in

a three-dimensional Poisson VD is  $(48\pi^2/35) + 2 \approx 15.535$ , with a standard deviation of 3.32 (Okabe et al. 2000).

To calculate the VD, we used the Quickhull algorithm (Barber, Dobkin & Huhdanpaa 1996), which runs in  $O(n \log n)$  time, where  $n$  is the number of input points. We also used the Qhull (the implementation of Quickhull) package to compute volumes of polyhedra. Because Qhull’s memory requirements become prohibitive when it is run directly on a large set of particles ( $\sim 10$  GB for a  $128^3$ -particle box), and also to produce intermediate outputs (valuable in interrupted runs), we split the box on which the VD is calculated into sub-boxes. A user constrained by memory may have to split the box into many pieces for them to fit into memory.

It is important to check that dividing the box does not alter particles’ volumes and sets of neighbors. See the appendix for details of how we do this.

## 2.2 Zones

We believe that the VD gives the best way of finding densities and adjacencies in a set of particles, and a prospective user of VOBOZ may wish to use it for this alone. Our method to group particles was more empirically found, but it does seem to work quite well in detecting even the smallest structures, and also in efficiently mapping out larger structures.

It is easy to define density maxima among particles given their densities and neighbors: a particle is a density maximum if its density is higher than any of its neighbors’. To find particles which may belong to that particle’s halo, we send each particle in the set to its neighbor with the highest density, and repeat this process until every particle is at a density maximum, a procedure similar to that in HOP. We define a density maximum’s *zone* to be the set of particles which jump to it; we define a zone’s *peak* to be its density maximum. Figure 2 shows this process.

However, we are far from finished with our analysis. In a Poisson VD, we found that 1/13.6 of the particles were density maxima. In our large-scale structure simulations, we typically found that about 1/19 of the particles were density maxima. This is not an overwhelming difference, so many of the density maxima seem to come from Poisson noise. ‘Zoning’ provides a convenient, fast partition of the set of particles, but zones can be oddly shaped, not necessarily resembling idealized mountains around peaks. This is for a few reasons: particles’ spatial positions are not explicitly considered in zoning, only their densities and adjacencies. Also, the fact that the peak of a particle’s zone lies on the steepest path up the density slope does not mean that there is no other zone to which the particle could conceivably belong. For example, if a particle is a local density minimum, it could be argued that its first jump could be to any of its neighbors. Many zones turn out to be fake, and the ones which lie at the centers of real haloes may contain far fewer particles than they should, because the haloes have been partitioned into many, often spurious, zones. However, we contend that it is a good thing to partition the particles into potential haloes in the finest (i.e. least coarse) possible way, which this arguably accomplishes.

It is therefore necessary to join some zones together; we do so referring to the following intuitive aid, illustrated in Fig. 3. Imagine that the particles occupy a two-dimensional surface with height given by their densities, enclosed in a

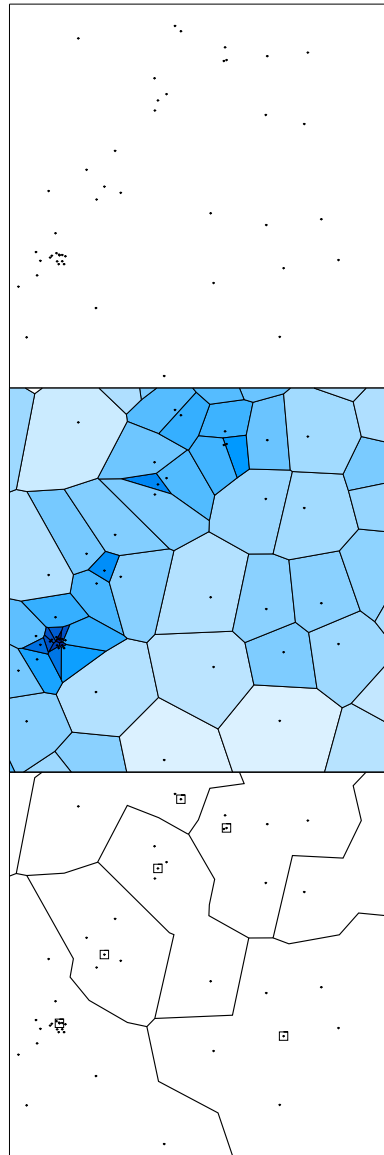


**Figure 2.** Zoning. The top panel shows a raw set of particles. The middle panel shows the 2-D Voronoi diagram of these particles, with cells shaded according to their areas. The bottom panel shows how these particles are partitioned into zones, with the peak of each zone indicated with a square.

water tank. We perform the following procedure for each zone  $z$ : Fill the tank until the peak of  $z$  is submerged, and then drain the water until a path emerges from the peak of  $z$  to the peak of another zone. The lowest-density particle on that path, with density  $\rho_{sl}$ , is the ‘strongest link’  $z$  has with any neighboring zone. The strongest link is the highest-density particle in the set of lowest-density particles on each path from the peak of  $z$  to the peaks of adjacent zones. In practice, this particle is quickly found, since we only need to search the border particles of each zone.

We continue adding adjacent zones to  $z$  until a zone joins whose peak exceeds  $z$ ’s in density; we call the end product a halo. The zones are not always joined one-at-a-time; to continue the analogy with the water tank, the strongest link density  $\rho_{sl}$  decreases monotonically, often uncovering

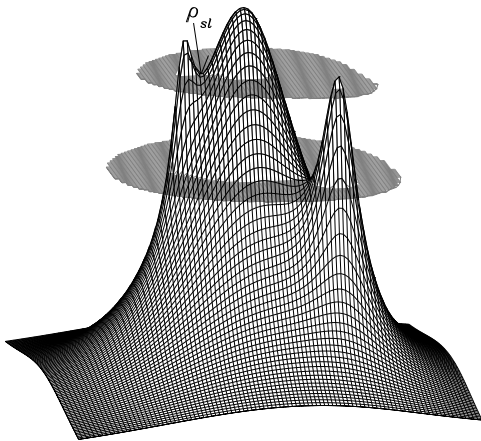


**Figure 3.** A schematic density field containing a halo with two subhaloes. If we put this surface in a water tank, and gradually reduce the water level, the central peak will be the first to emerge. As we reduce the water level, no higher peak is uncovered, so the entire region belongs to the central peak. If we reduce the water level from the peak of the left subhalo, we will reveal a landbridge to a higher peak when the water reaches the upper grey plane. If we do the same for the subhalo on the right, a landbridge to a higher peak will appear at the lower grey plane. We define the boundaries of each subhalo to be a density contour at the lowest density on the landbridge (at the height of its grey plane), called the strongest link density,  $\rho_{sl}$ . The probability that a subhalo is real depends on the ratio of its peak density to  $\rho_{sl}$ .

multiple zones at once. Thus, all zones connected to  $z$  by links with densities exceeding  $\rho_{sl}$  are considered as a single unit to merge with  $z$ , and the existence of one particle in this collection of zones with density higher than that of  $z$ 's peak will break the merger.

We have not yet discussed a criterion to halt the growth of large haloes well out into voids; without one, the zone with the densest particle in the simulation would grow to encompass the entire simulation. We tried to find some mathematical criterion to stop unambiguously at the edge of a halo, but had little success; everything we tried was easily tricked by complex geometries. One reason for the unbinding process, discussed in §2.3, is to mitigate this effect. Although there could exist a foolproof, parameter-free halo edge-detection method which has eluded us (and which, with any luck, will find its way into VOBOZ version 2.0), we reluctantly introduce a parameter  $\rho_{min}$  to limit the descent of  $\rho_{sl}$ , so that haloes do not grow across voids. The presence of a parameter is inherently undesirable, but it only affects the size of the largest haloes which are unquestionably present, and not the masses and identification of subhaloes, which is where the most headway is to be made in HFA's. We will discuss this parameter further in §3.1. We should also note that with haloes defined in this way, particles may belong to multiple haloes, e.g. to both a subhalo and its parent halo. While this is a matter of convention, we believe it is better to include subhaloes in the masses of their parents to which they gravitationally bound, and not to excise them simply because they are bound by themselves as well.

In other HFAs with Lagrangian density estimators like

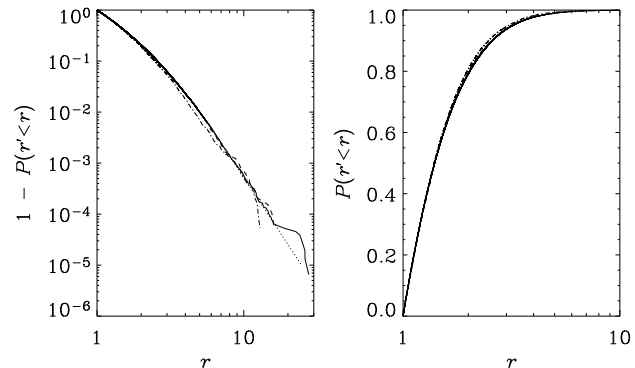


**Figure 4.** The cumulative probability function  $P(r' < r)$  of the ratio  $r(z)$  between the peak density of a zone and its critical strongest link density  $\rho_{sl}$ , from various Poisson simulations. The left panel shows  $1 - P(r' < r)$  on a logarithmic scale, while the right panel shows  $P(r' < r)$  on a more familiar linear scale on  $[0, 1]$ . The dashed curves are drawn from haloes in a uniform Poisson simulation with  $64^3$  particles, and the solid curves in one with  $128^3$  particles. The function does seem to converge as particle number increases. The dotted curve (indistinguishable in the right panel) shows the fit in Eqn. (1). The dot-dashed curve shows  $P(r' < r)$  of subhaloes in a large halo with density profile  $\rho \sim r^{-2}$ , Poisson sampled with  $64^3$  particles.

HOP, many spurious zones arise as in VOBOZ, but the problem is not directly addressed; zones are merely merged together if they exceed a density cut-off, and the substructure is forgotten. We use a different philosophy in VOBOZ: we measure for each halo or subhalo the probability that it exists, i.e. that it did not arise from Poisson noise.

This probability is judged according to the ratio  $r(z)$  of the peak density of  $z$  to the critical  $\rho_{sl}$  of the particle linked to a zone with a higher-density peak, halting  $z$ 's growth. We can turn this ratio into a probability by subjecting a Poisson set of particles to the same algorithm, and forming a cumulative distribution of its  $r(z)$ 's. The probability that a halo is real is then  $P(r) = P_{\text{Poisson}}(r' < r)$ , where  $P_{\text{Poisson}}$  is drawn from the Poisson realization. Figure 4 shows  $P(r)dr$ , the probability that a halo is fake as a function of its ratio  $r(z)$ . The dotted line in Fig. 4 is a fit we have made to  $P_{\text{Poisson}}(r' < r)$ :

$$1 - P_{\text{Poisson}}(r' < r) = \frac{1.077}{r^{1.82} + 0.077r^{4.41}} \quad (1)$$

Table 1 shows the ratios, calculated using Eqn. (1), which correspond to values of the standard Gaussian sigma:  $1\sigma$  corresponds to a probability of 68.3%,  $2\sigma$  to 95.4%,  $3\sigma$  to 99.7%, etc. By setting equal the two terms in the denominator of the fit expression, we find that there is a break where the power law steepens at  $r \approx 2.69$  ( $1.7\sigma$ ). This might then be a good candidate for a natural cut-off in  $r$  to separate real from fake haloes, with no reference to the type of data being analyzed. However, we do not recommend imposing a strict, *a priori* cut-off in  $r$ .

It might behoove us to test this fit with an even larger Poisson simulation, but it is academic to test whether a halo is fake with a  $10^{-4}$  or  $10^{-5}$  probability; the probabilities matter the most when a halo is questionable. It is perhaps more relevant to see what happens if a non-uniform distri-

**Table 1.** Ratios  $r(z)$  between a zone’s peak and its strongest link density, corresponding to probabilities  $P(r' < r)$ , calculated using Eqn. (1).

No. $\sigma$	$1 - P(r' < r)$	$r(z)$
0	1	1
1	0.317	1.69
2	$4.55 \times 10^{-2}$	3.30
3	$2.70 \times 10^{-3}$	6.82
4	$6.33 \times 10^{-5}$	16.3
5	$5.73 \times 10^{-7}$	47.3
6	$1.97 \times 10^{-9}$	171
7	$2.56 \times 10^{-12}$	773

bution (such as that in an  $N$ -body simulation) is Poisson-sampled. We put a single giant halo with a density profile  $\rho \sim r^{-2}$  in a periodic  $64^3$ -particle box by giving each particle a uniformly random distance to the center, and a uniformly random pair  $(\cos \theta, \phi)$  of angles. The cumulative  $r(z)$  distribution of the fake haloes detected in this simulation appears as the dot-dashed line in Fig. 4; the distribution is reassuringly similar to that from the uniform Poisson distribution.

### 2.3 Unbinding

We now have a set of prospective haloes defined using particles’ spatial positions. However, these prospective haloes may include particles which are not physically bound; for example, a portion of a nearby filament may be mistakenly included. We therefore test particles for boundness to their halo(es), for the first time introducing velocity information. For each halo, we compare the kinetic and potential energies of each particle, equivalent to comparing a particle’s velocity to its escape velocity. This does not always correctly predict whether the particle will be bound to the halo in the future, but it is a good estimate. The unbinding process is iterative, i.e. unbound particles are not included in the next iteration’s unbinding calculations for other particles.

Dividing out the mass of the particle, the kinetic energy of particle  $i$  is  $\frac{1}{2}|(\mathbf{v}_i - \mathbf{v}_c) + H(\mathbf{x}_i - \mathbf{x}_c)|^2$ , where  $\mathbf{v}_c$  is the velocity centroid of the original zone of the halo,  $H$  is the Hubble constant, and  $\mathbf{x}_c$  is the position of the central particle of the halo. We use the velocity centroid of only the original zone because VOBOZ sometimes joins together large regions which are unrelated in velocity space, which could skew the velocity centroid if the entire halo were included in the average. This is discussed further at the end of §3.3.

We calculate the potential at each particle  $i$  directly:

$$\Phi(\mathbf{x}_i) = G \sum_{j \neq i} \frac{M_j}{|\mathbf{x}_j - \mathbf{x}_i|}, \quad (2)$$

where  $j$  is summed over all bound particles in the halo, and  $M_j$  is the mass of the  $j$ th particle. However, for a halo with many particles, this direct,  $O(n^2)$  calculation of the potential for all particles is unwieldy. For this reason, we find shallower and deeper bounds for the potential which are calculable in less time. If a particle is bound in the shallower potential, it is bound in the real potential; if it is unbound in the deeper potential, it is unbound in the real one. The true potential is only calculated if the particle is unbound in the shallower potential but bound in the deeper one.

To get these bounds, we partition the halo on a three-dimensional grid with unequal spacing (see Fig. 5). In each

dimension, the grid spacing is set so that the number of particles in each one-dimensional bin is the same. In two dimensions, as in Fig. 5, this would mean that the number of particles in each row and column was the same. This does not guarantee that the same number of particles will be in each cell of the grid, but the particle counts in cells will certainly vary less than if we imposed a uniform grid, in which case the halo core would likely occupy only a couple of cells, decreasing the efficacy of the partition.

For the shallower bound to the potential of particle  $p$ , we calculate the potential produced by moving all other particles to the corners of their cells farthest from  $p$ . This potential is calculable in  $O(n)$  time because we only need to calculate the distance to a fixed (no dependence on  $n$ ) number of grid corners for each particle. For the deeper bound, we move all other particles to their cell corners closest to  $p$ , except for particles in the same cell as  $p$ , whose contributions to the potential are calculated directly. For each particle, the number of these particles requiring direct summation still scales with  $n$ , so in the worst case, the deeper bound still takes  $O(n^2)$  time. However, the constant multiplying  $n^2$  is much less than in the direct calculation. When deciding on the number of grid partitions, there is a tradeoff between accuracy of the upper and lower bounds and the time it takes to calculate them. The number of partitions should scale with the number of particles in the largest halo, since more accuracy will be required to capture all of its structure.

In analysing a large cluster (see §3.3), we found initially that our unbinding algorithm destroyed a few haloes which were visually evident, particularly when the full halo and not merely the core zone was used to calculate the velocity centroid. This happened because the haloes sent to the unbinding algorithm contained high-velocity particles which were not bound to the object, skewing the initial estimate of the velocity centroid and thus unduly unbinding particles which were needed to keep the halo together.

We addressed this problem by unbinding only the most unbound particles at each iteration, a technique suggested by Kravtsov (private communication). The only parameter-free way of doing this is to unbind only the most unbound particle at every iteration. We include code to do this with the VOBOZ package, even though it is cumbersome in practice since the binding energy for each bound particle must be recalculated each time. A time-saving alternative which we used is to set the threshold on boundness so that at first, only extremely unbound particles escape, but then to lower the threshold gradually to the right level. To do this, we find the most unbound particle, and set a multiplier  $m$  equal to the ratio of its kinetic to potential energy. The role of  $m$  is

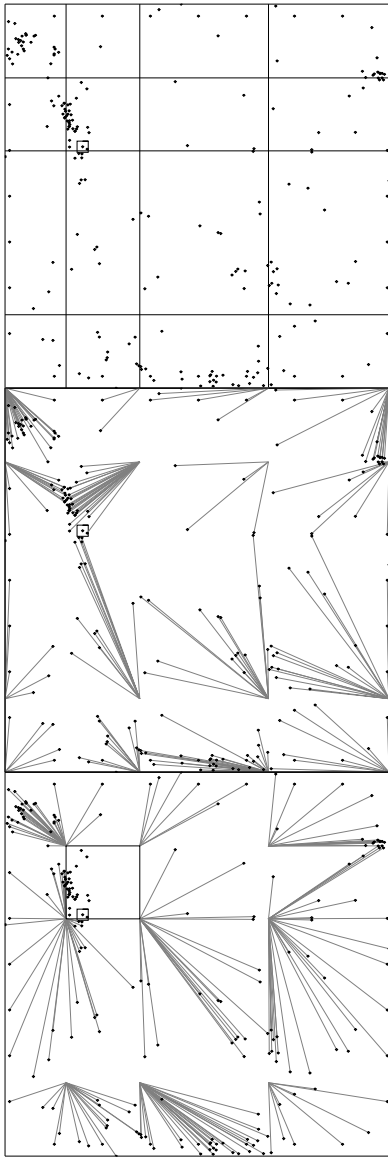


**Figure 5.** Our method to find the deeper and shallower bounds on the potential of a halo. The top panel shows a collection of particles, partitioned by a grid, spaced so that the number of particles in each row and column is the same. (This is only roughly true, of course, if the number of particles is not divisible by the number of rows or columns.) The true potential of the boxed particle  $p$  is found by directly summing the potentials from all other particles. The middle panel illustrates the method of finding the shallower bound, in which each particle is moved to the farthest corner in its cell from  $p$ . The bottom panel illustrates the deeper bound, in which each particle is moved to the nearest corner in its cell to  $p$ , except if it is in  $p$ 's cell, in which case its potential is directly summed.

to inflate the unbinding threshold artificially by multiplying the potential energy by it. Before each iteration, we reduce  $m$  by dividing it by a parameter  $f > 1$ , until  $m = 1$ , and the true unbinding criterion appears. The effects of changing  $f$  depend on the resolution and range of velocities in the simulation, and will be discussed in an extreme case in §3.3.

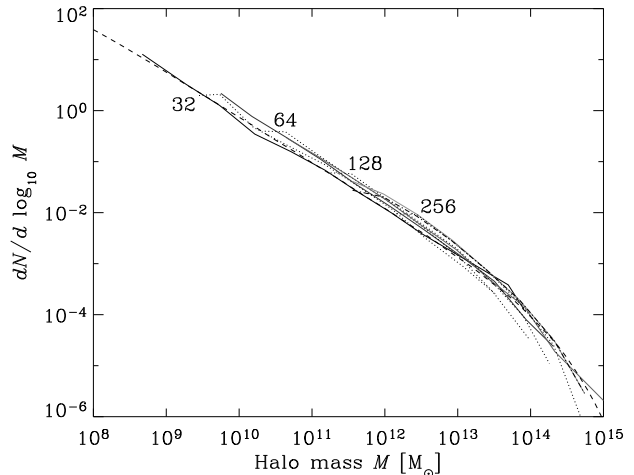


**Figure 6.** Mass functions of haloes from  $256^3$ -particle  $\Lambda$ CDM simulations, of box size 32, 64, 128, and  $256 h^{-1}$  Mpc. The solid curves show VOBOZ haloes, using a density cut-off  $\rho_{min}$  of 100. The dotted curves show haloes detected with DENMAX, using the canonical smoothing length of  $1/5$  the mean interparticle separation. The dashed line is the Sheth, Mo & Tormen (2001) analytical prediction.

### 3 TESTS

Using the NCSA p690 supercomputer, we applied VOBOZ to a set of nested  $256^3$ -particle  $\Lambda$ CDM simulations (described in NHG), with box sizes 32, 64, 128, and  $256 h^{-1}$  Mpc. We divided each simulation into two parts in each dimension; calculating the particle volumes and adjacencies took about one hour and 10 GB of RAM on each octant; it thus took about 8 hours total, trivially split on to 8 processors. The memory required can be reduced at the expense of processor time if the simulation is split into more pieces. The next step of the analysis was to join the zones together, which took, in all cases, about 6 minutes, and 3.2 GB of RAM. The time spent in the unbinding step depended greatly on the size of the haloes in the simulation, i.e. on the mass resolution and threshold density  $\rho_{min}$  (lower threshold densities give larger haloes). In the  $32 h^{-1}$  Mpc simulation, using  $f = \sqrt{2}$ , the unbinding step took from 4 to 65 processor-hours as  $\rho_{min}$  varied from 400 to 50; over the same range of  $\rho_{min}$ , the  $256 h^{-1}$  Mpc simulation took only from 1 to 4 hours. The amount of processor time also depends on the value of the unbinding delicacy parameter  $f$ . For the results below, we used  $f = \sqrt{2}$ . We did not check that this choice unbinds particles with maximal delicacy (which we did do for the cluster discussed in §3.3), but we do not expect the results of this simulation to saturate at values of the parameters as extreme as those for the cluster in §3.3, which has a higher velocity dispersion.

#### 3.1 Mass Functions

As Fig. 6 shows, the mass spectra of VOBOZ haloes from these simulations, using a density cut-off of  $\rho_{min} = 100$ , is roughly consistent with the Sheth, Mo & Tormen (2001) analytical mass function. While the mass function from the  $32 h^{-1}$

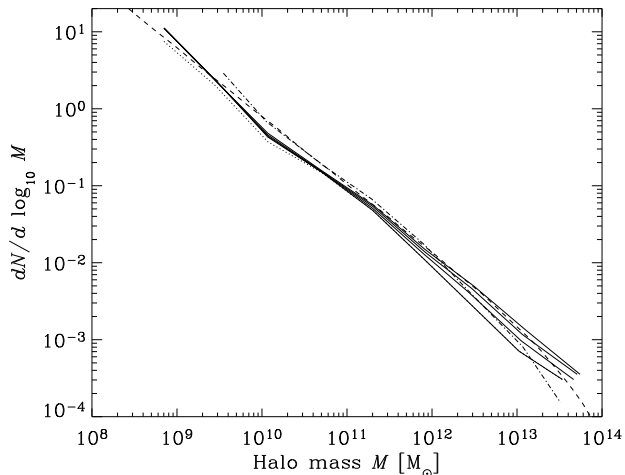


**Figure 7.** Mass functions of haloes from a  $256^3$ -particle  $\Lambda$ CDM simulation of box size  $32 h^{-1}$  Mpc. The solid curves show VOBOZ haloes, using density cut-offs  $\rho_{min}$  of (from top to bottom) 50, 100, 200, and 400. In the dotted curve, we weight each halo from the  $\rho_{min} = 400$  list by its probability; e.g. a 50% probable halo is counted as half a halo. The dot-dashed curve shows haloes from DENMAX, run with the canonical smoothing length of  $1/5$  the mean interparticle separation. The dashed line is the Sheth, Mo & Tormen (2001) analytical mass function.

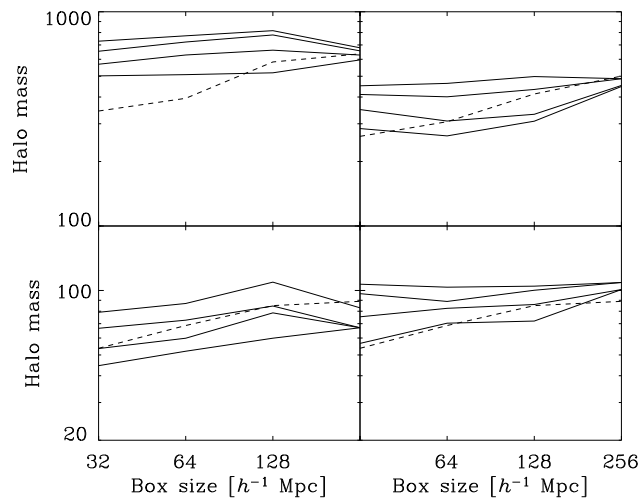


**Figure 8.** Dependence of halo mass on mass resolution for four haloes (one in each panel) identified through all four nested simulations described in NHG. The solid curves track the bound VOBOZ halo masses (in units of particle masses in the  $256 h^{-1}$  Mpc simulation, which is  $1.2 \times 10^{11} M_{\odot}$ ) in the four simulations using  $\rho_{min} = 50$  (top), 100 (bold), 200, and 400 (bottom). The lines should be horizontal if the haloes are identical and mass resolution does not affect the halo-finding. Particularly for large haloes, VOBOZ is much less sensitive to mass resolution than DENMAX. The discreteness of the zones making up the smallest (bottom row) haloes becomes apparent in the  $256 h^{-1}$  Mpc simulation, where the zones contain only  $\sim 100$  particles.

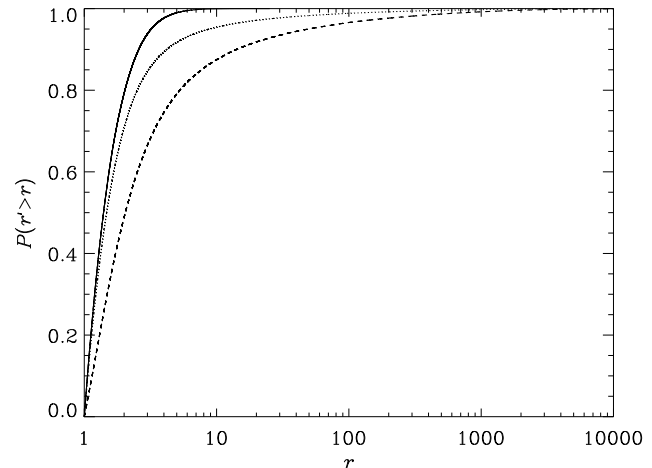


**Figure 9.** The cumulative distribution function of the ratio  $r(z)$  between the peak density of a zone and its critical strongest link density  $\rho_{sl}$ , from haloes in a uniform Poisson simulation (solid curve), from all haloes in the  $32 h^{-1}$  Mpc simulation (dotted), and from all bound haloes in this simulation (dashed).

Mpc simulation fits almost exactly, there is a systematic increase in the number of haloes of a given physical mass with box size. This also occurs, to a slightly lesser degree, in the DENMAX mass functions, indicating that it could arise from decreasing mass resolution in the simulations, and perhaps not from poor behavior by the HFA's.

The mass function does change with density cut-off  $\rho_{min}$ , but only significantly changes for the largest haloes. Figure 7 shows how the mass function of VOBOZ haloes in the  $32 h^{-1}$  Mpc simulation changes as  $\rho_{min}$  varies from 400 to 50. Generally, the number of low-mass haloes stays fixed; the main effect of this parameter is on the slope of the mass function.

It is also useful to see how VOBOZ mass varies with mass resolution. In NHG, we identified four haloes present in all of the nested 32, 64, 128, and  $256 h^{-1}$  Mpc simulations we ran. Figure 8 shows their masses (normalized to the particle mass in the  $256 h^{-1}$  Mpc simulation) as a function of box size (and, therefore, mass resolution), for four different values of  $\rho_{min}$ . For all values of  $\rho_{min}$ , VOBOZ returned a halo mass less dependent on mass resolution than did DENMAX. For the canonical density cut-off,  $\rho_{min} = 100$  (the bold line in all panels), the mass of the halo changed little with box size.

We had hoped that the unbinding criterion would take away the dependence on  $\rho_{min}$ , and that as the density cut-off  $\rho_{min}$  is decreased, the bound mass of a large halo would plateau. However, adding any particles to a halo deepens its potential well, feeding back positively on the number of particles possibly bound to it. Thus, the bound mass of an isolated halo usually rises unchecked with the pre-unbinding mass. The unbinding test is still quite necessary, however, to eliminate haloes whose high velocity dispersions render them evanescent. From the 16,777,216 particles in the  $32 h^{-1}$  Mpc simulation, 876,592 peak particles, and thus zones, were detected; on average, one in every 19 particles was a peak. The unbinding step reduced the number of haloes to

about 280,000 ( $\pm 800$  as  $\rho_{min}$  varied from 50 to 400). In the  $256 h^{-1}$  Mpc simulation, 900,139 zones were detected, out of which  $618,100 \pm 100$  were bound. It is not surprising that more bound structures were detected in the simulation encompassing the larger physical volume. Figure 9 shows the cumulative distribution of the ratio  $r$  of peak density to strongest link density for all haloes and all bound haloes in the  $32 h^{-1}$  Mpc simulation, using  $\rho_{min} = 100$ . At the low-probability end, the CDF of pre-unbinding haloes (the dotted curve) tracks the CDF from the Poisson simulation, but the CDF of bound haloes (the dashed curve) departs from the Poisson curve, indicating that many of the least probable haloes are not bound. This supports our claim that  $r$  is a good tracer of halo probability.

### 3.2 Correlation Functions

Because there is no resolution limit in VOBOZ, we expected to, and did, find pairs of haloes much closer together than in the algorithm we previously applied to this simulation, DENMAX<sup>2</sup> (see NHG). In DENMAX<sup>2</sup>, DENMAX is run as usual, and then is run again, with half the canonical smoothing length, on each halo from the previous run to resolve subhaloes. Figure 10 shows the correlation functions (CFs) of sets of haloes characterized by cut-offs in probability (assigned using the ratio  $r$ ), compared to the CF of all DENMAX<sup>2</sup> haloes. DENMAX<sup>2</sup> imposes a strict 10-particle minimum; the DENMAX<sup>2</sup> haloes are larger and therefore have higher CFs. We also measured the total CF of haloes, weighting pairs of haloes by the product of their probabilities; this total CF is close to the unweighted CF of all (without a probability cut-off) haloes. We should note that these CFs are lower in amplitude than are observed galaxy CFs, which stems from the inclusion of even the smallest, two-particle haloes in the simulation, which have a mass of  $5 \times 10^8 M_\odot$ . The population of DENMAX<sup>2</sup> haloes from this simulation which best fit the PSCz power spectrum (NHG) had at least 800 particles.

Figure 10 shows another trend as we vary the probability cut-off, written in terms of the standard Gaussian  $\sigma$ . Starting from a high probability cut-off and decreasing it to allow in more dubious haloes, a ‘hook’ rises in the CF at low radius. This says that the closest pairs include at least one low-probability halo, which makes sense by our definition of probability: a low-probability peak has a shallow, and most likely short, landbridge to another, denser peak. At the same time, the CF decreases at high separation when improbable haloes are added, because they are also generally smaller, and therefore more weakly clustered. Interestingly, the radius separating these two regimes is relatively constant for plausibly low values of  $\sigma$ , producing a nexus (here, at about  $0.1 h^{-1}$  Mpc) where CFs cross. It is tempting to interpret the ‘hook’ at low radius as a ‘1-halo’ or ‘Poisson’ term (e.g. Zehavi et al. 2004) in the galaxy CF, consisting of pairs of galaxies (i.e. subhaloes) within the same halo.

To test this hypothesis, we tried to use a probability cut-off to produce a ‘2-halo’ term obtained explicitly using the halo model formalism from an  $N$ -body simulation. Kravtsov et al. found the 2-halo contribution to the CF of haloes (and subhaloes) exceeding  $10^{12} h^{-1} M_\odot$  in an  $80 h^{-1}$  Mpc simulation, which appears in their Fig. 8. In our Fig. 11, we show CFs of all haloes from our 64, 128, and  $256 h^{-1}$  Mpc simulations (black curves), along with attempts at 2-halo

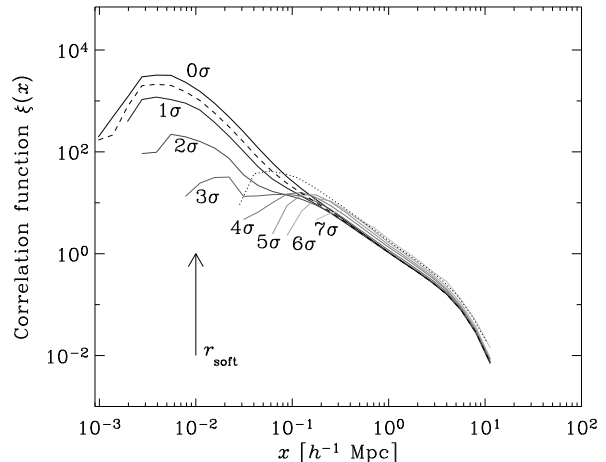


**Figure 10.** Correlation functions (CFs) of haloes from a  $256^3$  particle,  $32 h^{-1}$  Mpc  $\Lambda$ CDM simulation, with softening length  $r_{soft} = 0.01 h^{-1}$  Mpc. The solid lines are labeled with their probability cut-offs, ranging from  $1 - 7\sigma$ . The dashed line is a CF of all VOBOZ haloes, weighting pairs by the product of their probabilities. There is no cut-off imposed in halo size, so the smallest haloes included have only two particles, giving a minimum halo mass of  $5 \times 10^8 M_\odot$ . The dotted curve is the CF of all DENMAX<sup>2</sup> haloes with greater than 10 particles, i.e. with a minimum mass of  $2 \times 10^9 M_\odot$ .

terms (grey curves). To obtain the 2-halo term, we varied a probability cut-off in increments of  $\sigma$  to get the CF to turn away from the full CF at about  $1 h^{-1}$  Mpc, where Kravtsov et al. found that their 1-halo and 2-halo terms cross. The probability cut-offs for the CFs shown are  $4\sigma$ ,  $6\sigma$ , and  $7\sigma$  for the 256, 128, and  $64 h^{-1}$  Mpc simulations, respectively. This supports the idea that halo probability is a measure of a halo’s ‘sub-haleness,’ although the cut-off at which full ‘haleness’ occurs varies with mass resolution, and is likely somewhat fuzzy. Another thing to point out is that the scale of the inflection indicating the onset of the CF 1-halo term increases with the size of the halo sample; as Figs. 10 and 11 show, the scale of the inflection increases by a factor of ten as the mass cut-off is raised from  $5 \times 10^8 M_\odot$  to  $10^{12} h^{-1} M_\odot$ .

We should also note that in Fig. 11, the CFs of haloes exceeding the same physical mass from three simulations of different box size and mass resolution coincide over a wide range of scales, a concordance which we could not achieve in NHG using DENMAX mass. This boosts our confidence in VOBOZ’s mass estimate.

### 3.3 A Large Cluster

We have claimed that VOBOZ is adept at finding small structures in simulations; to test this claim, we have applied it to a large, high-resolution cluster of mass a few times  $10^{14} h^{-1} M_\odot$ , provided by Andrey Kravtsov. It was drawn from a simulation appearing in Tasitsiomi et al. (2004), which has a box size of  $80 h^{-1}$  Mpc, and a particle mass ranging from  $3.159 \times 10^8 h^{-1} M_\odot$  to 64 times that. The simulation was designed so that the smallest particles would end up in clus-



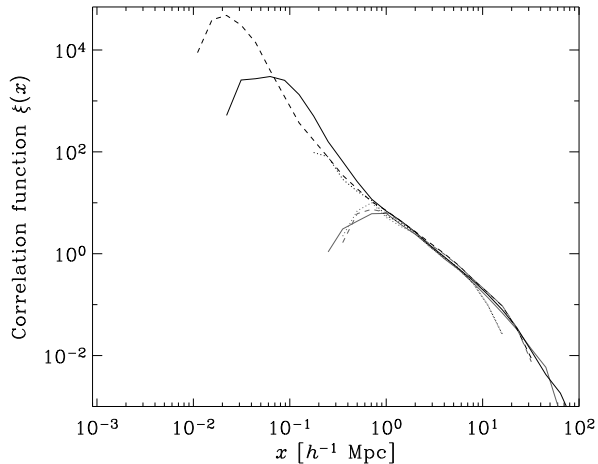


**Figure 11.** An attempt to use a probability cut-off to isolate the ‘2-halo’ term in the correlation function (CF) of haloes exceeding  $10^{12} h^{-1} M_{\odot}$  in our 256 (solid), 128 (dashed), and 64 (dotted)  $h^{-1}$  Mpc simulations. The black curves are CFs of all haloes, while the grey curves are CFs of haloes exceeding probability cutoffs of  $4\sigma$ ,  $5\sigma$ , and  $6\sigma$  in the 256, 128, and 64  $h^{-1}$  Mpc simulations, respectively. (C.f. Kravtsov et al. 2004, Fig. 8)

ters such as this one. We ran VOBOZ only on these smallest particles, which comprised over 99% of the mass at all radii out to  $2 h^{-1}$  Mpc from the cluster core. In the following analysis, we considered only haloes within this radius.

In this region with a high velocity dispersion, it was necessary to unbind particles delicately, unbinding only the most unbound particles at every iteration. As described at the end of §2.3, we did this by gradually decreasing a factor multiplying the potential energy until the true unbinding criterion is left. Figure 12 shows how the number of haloes detected depends on the unbinding coarseness parameter  $f$  (the factor by which the potential multiplier is divided at each iteration). Indeed, it saturates when  $f$  is sufficiently small, which probably arises from particle discreteness, since only one particle can be unbound at a time. We recommend using a reasonably small value of  $f$ , but it does not matter much if  $f$  moderately exceeds the saturation point, since most of the haloes missed with a large choice of  $f$  have low probability. One might also wonder how the masses of robust haloes changes with  $f$ ; with a couple of exceptions, they change not at all, or only negligibly. For the results discussed below, we used  $f = \sqrt[128]{2}$ . A simulation without as high a velocity dispersion would likely accommodate a larger value of  $f$ . We used an extremely low density cut-off  $\rho_{min} = 1$ , so that the only halo which would be affected by  $\rho_{min}$  would be the cluster itself.

Figure 13 shows the mass function of haloes in this cluster returned by both VOBOZ and a variant (Kravtsov et al. 2004) of BDM. The BDM halo list was produced by Kravtsov, analysing only the smallest particles in the cluster as we did. The mass functions from both algorithms agree reassuringly well, except at the low-mass end, where VOBOZ detects far more haloes (if we apply no probability cut-off). However, these are also the most improbable haloes, as illustrated by the descent of the solid curves with increasing probability

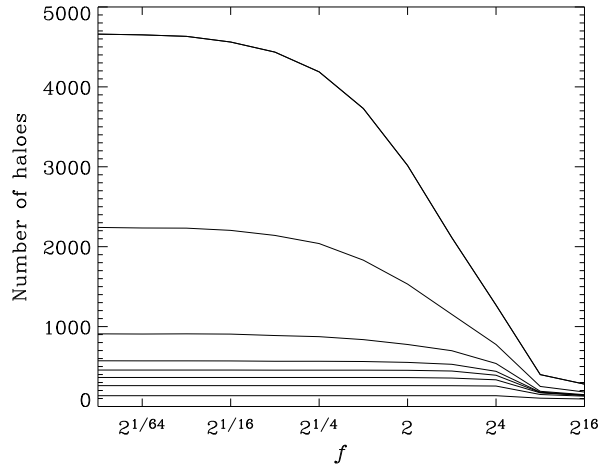


**Figure 12.** Effect of unbinding coarseness on the number of haloes VOBOZ finds in a large cluster. The curves show the number of haloes satisfying various probability cut-offs, from  $0\sigma$  (top) to  $7\sigma$  (bottom). As  $f$  (the factor by which the potential multiplier is divided at each iteration) increases, so does the number of low-probability haloes that VOBOZ completely unbinds.

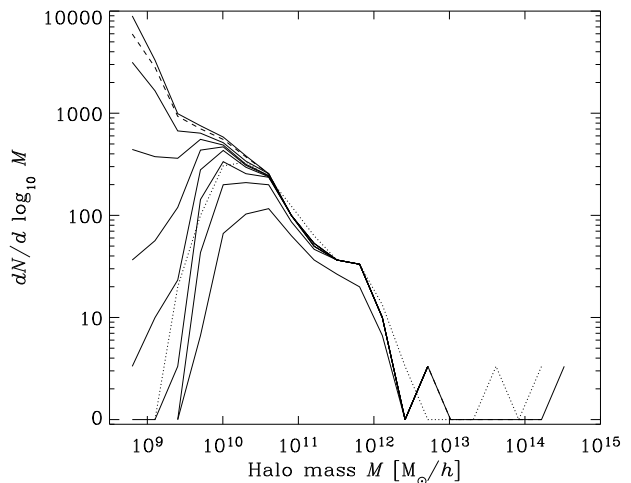


**Figure 13.** Mass function of haloes from a large cluster. The dotted curve shows haloes found by a variant of BDM. The solid curves show VOBOZ haloes satisfying various probability cut-offs. The top (first) solid curve applies no cut-off, and the second applies a cut-off of  $1\sigma$ ; the probability cut-off increases in increments of  $\sigma$  down to the bottom curve, where it reaches  $7\sigma$ . The dashed curve weights each halo with its probability. The odd behavior at high  $M$  arises from differing masses returned by the two HFAs for the two largest haloes.

cut-off. We also tried to match haloes detected by both algorithms in a rather crude fashion: for each BDM halo, we formed a list of all VOBOZ haloes within  $0.02 h^{-1}$  Mpc of it, which is a bit under twice the separation between the cluster core as detected by VOBOZ and the core as detected by BDM. We declared the matching VOBOZ halo to be the one with the nearest mass on a logarithmic scale within this sphere. This

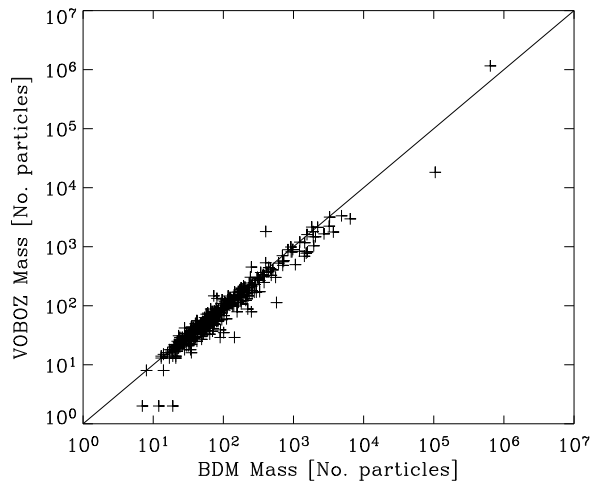


**Figure 14.** Scatter plot of masses, in units of particle mass, of haloes detected by both a variant of BDM, and VOBOZ. The line shows where the masses should lie if the HFAs returned identical masses. A VOBOZ halo may be matched with many BDM haloes. The largest halo is the cluster itself, which included many larger-mass particles in the actual simulation, so its mass is underestimated by both algorithms.

method is ‘rather crude’ because one VOBOZ halo can match several BDM haloes. Out of 383 BDM haloes, 5 small ones did not have VOBOZ neighbors within the search radius. Figure 14 shows a scatter plot of the masses of matching haloes, which is again reassuring.

Our method of joining together zones is designed for the idealized situation of Fig. 3. However, when it is applied to a collection of middling haloes with a background density above the cut-off, the halo which happens to have the highest-density core particle can acquire unwelcome neighbors. Figure 15 shows an extreme case of this phenomenon, taken from the Kravtsov cluster. All of the visually evident subhaloes pass the  $4\sigma$  test, but the probability we assign may start to lose its meaning by  $7\sigma$ , since the most obvious subhalo does not exceed this probability. The ‘halo’ pictured here has perhaps more structure in velocity space than in position space, suggesting that an ideal HFA would search for clusters in 6-D position-velocity space. Such a thing could separate two colliding haloes, which, in the worst case, VOBOZ would identify as a single halo, and then perhaps unbind completely because of its bimodal velocity distribution. In the mean time, the unbinding method we use seems to work fairly well in picking out structures in velocity space.

Figure 15 also illustrates the need to average together only the velocities in the central zone of a halo to find the velocity centroid used in unbinding. With the velocity centroid defined in this way, the same set of particles was returned as bound for all values of the unbinding delicacy parameter  $f$ . On the other hand, using the entire halo to determine the velocity centroid, we obtained results which depended strongly on  $f$ . Sometimes, we would obtain the right answer (the halo around the central zone); sometimes, another halo would be returned (resulting in double counting in the halo catalog); and sometimes, all particles would be unbound.

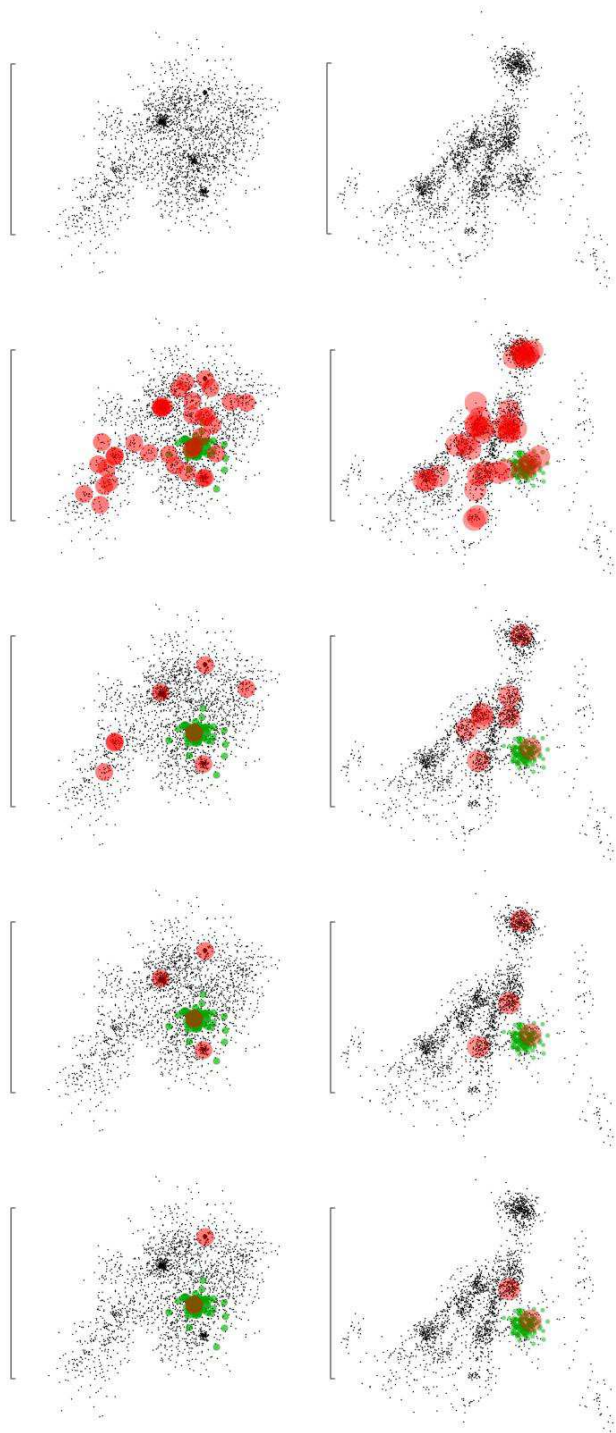


**Figure 15.** A particularly messy ‘halo’ in a large cluster. On the left, the ‘halo’ is shown in position space (with a  $0.8 h^{-1}$  Mpc bracket); on the right, it is shown in velocity space (with a 1000 km/s bracket). The black dots represent all particles in the ‘halo,’ including those eventually unbound; the raw particles appear in the first row. In subsequent rows, those particles which VOBOZ deems bound to the final halo are replaced with bloated green particles. In position space, the large red circles show the centers of haloes which lie within this larger ‘halo,’ in velocity space, the circles show their velocity centroids. The second row shows all haloes; the third row shows all haloes with probabilities above  $2\sigma$ ; the fourth shows haloes above  $4\sigma$ ; and the bottom shows haloes above  $7\sigma$ . This figure was produced using Nick Gnedin’s IFRIT visualization tool, at <http://casa.colorado.edu/~gnedin/IFRIT/>.

## 4 CONCLUSION

We have developed a halo-finding algorithm, called VOBOZ, which is nearly parameter-free, and which has a resolution limited only by the discreteness of particles in the simulation it is analysing. The Voronoi diagram allows us to fix the densities and the sets of neighbors for all particles in a ‘natural,’ parameter-independent way, on arguably the finest possible scale that contains meaningful structure. Further degrees of freedom are eliminated by assigning to each halo (or sub-halo) a probability that it exists, i.e. that it did not arise from Poisson noise.

Of the two parameters in VOBOZ, one of them exists only to save processor time, and needs not be used if one has no processor time constraints. This parameter controls the delicacy with which particles are unbound, and the results saturate at the ‘right’ answer (the parameter-free situation in which one particle is unbound at a time) when the unbinding becomes sufficiently delicate. Additionally, most of the extra haloes uncovered at extreme delicacy have meager probabilities. The remaining parameter is a density cut-off, necessary because haloes do not extend to low densities in the real universe. However, it only affects the masses of the largest haloes in the simulation, and not the masses or detection of subhaloes, which is where reliability in halo-finding algorithms is most needed.

An ideal halo-finding algorithm would find groups of particles in both position and velocity space, or even consider neighboring time slices in a simulation. In VOBOZ, the velocities are used only to decide if particles are energetically bound to haloes found in position space. This is an approximate criterion, but it seems to work acceptably well.

The probability VOBOZ returns for each halo is certainly tied to the finite mass resolution of the simulation it is analysing. However, as we decrease a cut-off in halo probability, an interesting signal emerges in the halo correlation function which resembles the 1-halo term in the halo model of large-scale structure. This suggests an interpretation of halo probability as a measure of a halo’s ‘sub-haleness,’ which may increase VOBOZ’s appeal for researchers of the halo model.

The VOBOZ code is publically available, at <http://casa.colorado.edu/~neyrinck/voboz/>.

## ACKNOWLEDGMENTS

We thank Andrey Kravtsov for enlightening discussions, and for providing us with cluster data to analyze, without which we would not have realized how delicately haloes must be unbound. We also thank Rien van de Weygaert for a helpful referee’s report. This work was supported by NASA ATP award NAG5-10763, NSF grant AST-0205981, and a grant by the National Computational Science Alliance.

## REFERENCES

Arad I., Dekel A., Klypin A., 2004, MNRAS, submitted. (astro-ph/0403135)  
 Barber C.B., Dobkin D.P., Huhdanpaa H.T., 1996, ACM Transaction on Mathematical Software, 22, 469  
 Berlind A.A., Weinberg D.H., 2002, ApJ, 575, 587

Bertschinger E., Gelb J.M., 1991, Computers in Physics, 5, 164  
 Davis M., Efstathiou G., Frenk C., White S.D.M., 1985, ApJ, 292, 371  
 Eisenstein D.J., Hut, P., 1998, ApJ, 498, 137  
 Ebeling H., Wiedenmann G. 1993, Phys. Rev. E 47, 704  
 Icke V., van de Weygaert R., 1987, A&A, 184, 16  
 Jang-Condell H., Hernquist L., 2001, ApJ, 548, 68  
 Kim J., Park C., 2004, ApJ, submitted. (astro-ph/0401386)  
 Kim R.S.J., et al., 2002, AJ, 123, 20  
 Klypin A.A., Holtzman J., 1997, preprint (astro-ph/9712217)  
 Kravtsov A.V., Berlind A.A., Wechsler R.H., Klypin A.A., Gottlöber S., Allgood B., Primack J.R., 2004, ApJ, 609, 35  
 Marinoni C., Davis M., Newman J., Coil A., 2002, ApJ, 580, 122  
 Neyrinck M.C., Hamilton A.J.S., Gnedin N.Y., 2004, MNRAS, 341, 1  
 Okabe A., Boots B., Sugihara K., Chiu S.N., 2000, Spatial Tessellations (New York: Wiley)  
 Pelupessy F.I., Schaap W.E., van de Weygaert R., 2003, A&A, 403, 389  
 Ramella M., Boschin W., Fadda D., Nonino M., 2001, A&A, 368, 776  
 Schaap W.E., 2004, PhD thesis, Univ. of Groningen  
 Schaap W.E., van de Weygaert R., 2000, A&A, 363, 29  
 Sheth R.K., Mo H., Tormen G., 2001, MNRAS, 323, 1  
 Tasitsiomi A., Kravtsov A.V., Gottlöber S., Klypin A.A., 2004, ApJ, 607, 125  
 van de Weygaert R., 1994, A&A, 283, 361  
 Voronoi G., 1908, J. Reine Agnew. Math., 134, 198  
 Weinberg D.H., Hernquist L., Katz N., 1997, ApJ, 447, 8  
 Zehavi, I., et al., 2004, ApJ, 608, 16

## APPENDIX A: GUARDING SUB-BOXES

To check that dividing the simulation box does not alter its Voronoi diagram, we surround each sub-box with a buffer zone large enough to contain all of the neighbors of the particles inside the sub-box. Figure A1 shows a sub-box surrounded by a buffer. We have deployed guard particles, shown as diamonds, inside the buffer. If one of the guard particles is returned as a neighbor to a sub-box particle, then it is possible that the sub-box particle has a neighbor outside the buffer, and we must recalculate the VD on the sub-box with a larger buffer.

The distance  $g$  between the sub-box and the guard particles is determined as follows. The guard particles are arranged inside each face of the buffer, of width  $b$ , on two dimensional grids with spacing  $s$ . Figure A2 shows two diagonally adjacent (and thus separated by a distance  $s\sqrt{2}$ ) guard particles, shown as diamonds. We want the guard particles to ‘catch’ any sub-box particles for which a particle outside the buffer could affect its Voronoi cell. The worst-case scenario, in which the guard particles have the least guarding power, occurs if there is a particle right on the border of the sub-box, where the square is. The closest possible point to the square outside the buffer is the triangle. If the triangle is in the square’s set of neighbors (but is artificially excluded because it lies outside the buffer), then so will a guard point if the perpendicular bisector (a dotted line) between that guard point and the square intersects the line segment between the triangle and square at its midpoint (the confluence of the three lines of length  $b/2$ ), or nearer to the square than the triangle. So the guard points must be placed on a sphere with radius  $b/2$ , tangent to both the

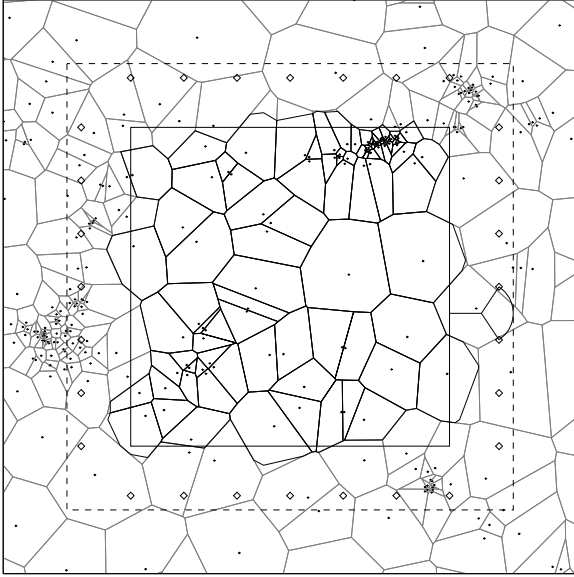


**Figure A1.** The same region as in Figure 1, with a Voronoi diagram on a sub-box superimposed. Solid lines demarcate the sub-box, with the buffer around it outlined by dashed lines. Guard points in the buffer appear as diamonds. The Voronoi cells calculated using all particles appear in grey, while the Voronoi cells of particles in the sub-box calculated using only the sub-box, buffer, and guard particles appear in black. There are a few discrepancies, notably at the center on top, and on both sides near the bottom. Discrepancies indicate that the buffer should be enlarged, and the VD recalculated.

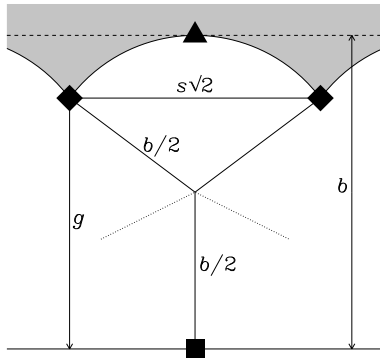


**Figure A2.** A diagram showing the calculation of  $g$ , the optimal distance from the sub-box (at the bottom of the diagram) to the guard points. The guard points preempt alteration of the sub-box Voronoi diagram, ensuring that points outside the buffer, of width  $b$ , cannot affect it. The diamonds are guard points diagonally adjacent on a two-dimensional grid of spacing  $s$ , offset by a distance  $g$  from a face of the sub-box. The hardest scenario for the guard points to preempt has a particle in the sub-box at the square, and a particle outside the buffer at the triangle, which would have been one of the square's neighbors if it were inside the buffer. The guard points preempt any potential neighbors to the square which lie in the shaded region. The dotted lines are perpendicular bisectors between the diamonds and the square.

buffer and sub-box boundaries. This leads to an equation for the largest-possible  $g$ :

$$g = \frac{b}{2} \left( 1 + \sqrt{1 - \frac{2s^2}{b^2}} \right). \quad (\text{A1})$$

As the number of guard points increases,  $s$  decreases, which moves  $g$  toward the edge of the buffer. Thus, increasing the number of guard points can provide an alternative to increasing the buffer size if guard points are encountered in the tessellation, but only if the buffer truly contains all of the neighbors of points inside the sub-box.